Early adolescent Rai1 reactivation reverses transcriptional and social interaction deficits in a mouse model of Smith–Magenis syndrome

Wei-Hsiang Huang[a,b,1], David C. Wang[a,b], William E. Allen[a,c], Matthew Klope[d], Hailan Hu[e,f], Mehrdad Shamloo[d,g], and Liqun Luo[a,b,c,1]

[a]Howard Hughes Medical Institute, Stanford University, Stanford, CA 94305; [b]Department of Biology, Stanford University, Stanford, CA 94305; [c]Neurosciences Program, Stanford University, Stanford, CA 94305; [d]Stanford Behavioral and Functional Neuroscience Laboratory, Stanford University School of Medicine, Stanford, CA 94305; [e]Interdisciplinary Institute of Neuroscience and Technology, Zhejiang University, 310012 Hangzhou, People's Republic of China; [f]Qiushi Academy for Advanced Studies, Zhejiang University, 310012 Hangzhou, People's Republic of China; and [g]Department of Neurosurgery, Stanford University School of Medicine, Stanford, CA 94305

Contributed by Liqun Luo, August 24, 2018 (sent for review April 20, 2018; reviewed by Guoping Feng and Daniel H. Geschwind)

Haploinsufficiency of *Retinoic Acid Induced 1* (*RAI1*) causes Smith–Magenis syndrome (SMS), a syndromic autism spectrum disorder associated with craniofacial abnormalities, intellectual disability, and behavioral problems. There is currently no cure for SMS. Here, we generated a genetic mouse model to determine the reversibility of SMS-like neurobehavioral phenotypes in *Rai1* heterozygous mice. We show that normalizing the Rai1 level 3–4 wk after birth corrected the expression of genes related to neural developmental pathways and fully reversed a social interaction deficit caused by *Rai1* haploinsufficiency. In contrast, *Rai1* reactivation 7–8 wk after birth was not beneficial. We also demonstrated that the correct Rai1 dose is required in both excitatory and inhibitory neurons for proper social interactions. Finally, we found that *Rai1* heterozygous mice exhibited a reduction of dendritic spines in the medial prefrontal cortex (mPFC) and that optogenetic activation of mPFC neurons in adults improved the social interaction deficit of *Rai1* heterozygous mice. Together, these results suggest the existence of a postnatal temporal window during which restoring Rai1 can improve the transcriptional and social behavioral deficits in a mouse model of SMS. It is possible that circuit-level interventions would be beneficial beyond this critical window.

autism spectrum disorders | copy number variation | chromatin | social behavior | Smith–Magenis syndrome

Genomic disorders are common conditions (1 in 1,000 births) caused by chromosomal instability and copy number variation that result in structural variations of DNA fragments (1). While the pathology is often driven by dosage imbalance of multiple genes, sometimes a single dosage-sensitive gene is responsible for the majority of phenotypes (1). One such example is Smith–Magenis syndrome (SMS), a neurodevelopmental disorder frequently diagnosed in infancy or early childhood due to hypotonia and dysmorphic features (2). With age, SMS patients display neurological features including cognitive impairment, self-injurious behaviors, and stereotypies (2). Most SMS patients (>90%) meet criteria for autism spectrum disorder (ASD) at some point in their lives (3). Ninety percent of SMS patients harbor chromosomal deletions in 17p11.2 (4), while the remaining 10% have point mutations or small deletions in *Retinoic Acid Induced 1* (*RAI1*), which resides in 17p11.2 (4, 5). Phenotypic comparison between patients with 17p11.2 deletions and *RAI1* mutations demonstrated that most SMS features are a result of *RAI1* haploinsufficiency (6). Importantly, an increased RAI1 level may contribute to Potocki–Lupski syndrome (PTLS), a neurodevelopmental disorder characterized by 17p11.2 duplication and high prevalence of ASD (>60%) (7, 8). Although *RAI1* is among the dozens of genes overexpressed in PTLS, the smallest region common to PTLS patients with different duplications is a 125-kb region containing only *RAI1* (9). Therefore, the nervous system is sensitive to *RAI1* dosage. Currently, no cure is available for SMS or PTLS patients. Treatments of symptoms with neuroleptics, antipsychotics, and serotonin reuptake inhibitors demonstrate limited success at the cost of significant adverse effects (10, 11).

Rai1 encodes a chromatin-binding protein that regulates the expression of many neurodevelopmental genes in the mammalian brain (12). It is thus difficult to develop a therapeutic strategy that simultaneously targets multiple Rai1 downstream pathways. In mice, *Rai1* begins to express at embryonic day 9.5 and is continuously expressed throughout adulthood (12, 13). Most $Rai1^{-/-}$ mice die as embryos (13), demonstrating that Rai1 is essential during early embryonic development. Therefore, it is possible that SMS symptoms are a consequence of irreversible damage to neural functions resulting from the absence of *Rai1* during early development. However, *Rai1* is continuously expressed in the adult brain (12), suggesting that Rai1 function may also be required beyond development. If true, it is possible that postnatal restoration of a normal *Rai1* expression level may improve neural functions and reverse SMS symptoms. To distinguish between these possibilities, we combined genetic- and circuit-level interventions to correct SMS-like transcriptional and neurobehavioral phenotypes in mice.

Significance

Losing one copy of the *RAI1* gene causes Smith–Magenis syndrome (SMS), a neurodevelopmental disorder. Using a newly generated SMS mouse model, this study demonstrates that restoring the *Rai1* gene dose in an early postnatal window could repair gene expression and social interaction deficits in this SMS model. The SMS mouse model also showed a reduced density of dendritic spines, anatomical correlates of excitatory synapses, in the prefrontal cortex. Artificial activation of prefrontal cortex neurons partially alleviated the behavioral deficits. These findings suggest that, similar to Rett syndrome, SMS is caused by disruption of a chromatin-modifying gene with reversible developmental phenotypes, highlighting the potential treatment windows in childhood or adolescence.

Author contributions: W.-H.H., H.H., and L.L. designed research; W.-H.H., D.C.W., and M.K. performed research; W.-H.H. contributed new reagents/analytic tools; W.-H.H., D.C.W., W.E.A., M.K., M.S., and L.L. analyzed data; and W.-H.H. and L.L. wrote the paper.

Reviewers: G.F., Massachusetts Institute of Technology; and D.H.G., University of California, Los Angeles.

The authors declare no conflict of interest.

[1]To whom correspondence may be addressed. Email: weihsiah@stanford.edu or lluo@stanford.edu.

This article contains supporting information online at www.pnas.org/lookup/suppl/doi:10.1073/pnas.1806796115/-/DCSupplemental.

Published online October 1, 2018.

Results

An SMS Mouse Model That Allows Conditional Reactivation. To test reversibility of SMS in mice, we generated a knock-in *Rai1* allele ($Rai1^{STOP}$) with an insertion of a *loxP*-flanked transcriptional stop cassette before the start codon, which should prevent the expression of any Rai1 protein before Cre-mediated recombination (Fig. 1*A* and *SI Appendix*, Fig. S1*A*). We found that, similar to $Rai1^{-/-}$ mice (13), most $Rai1^{STOP/STOP}$ mice died in utero (91%, $n = 175$), suggesting that $Rai1^{STOP}$ functions as a null allele in the absence of Cre activity. Quantitative RT-PCR and Western blot confirmed that the stop cassette effectively inhibited the expression of *Rai1* (Fig. 1 *B* and *C*). We then performed a battery of behavioral assays using 8- to 10-wk-old male $Rai1^{STOP/+}$ mice and their wild-type (WT) littermates to examine their neural functions.

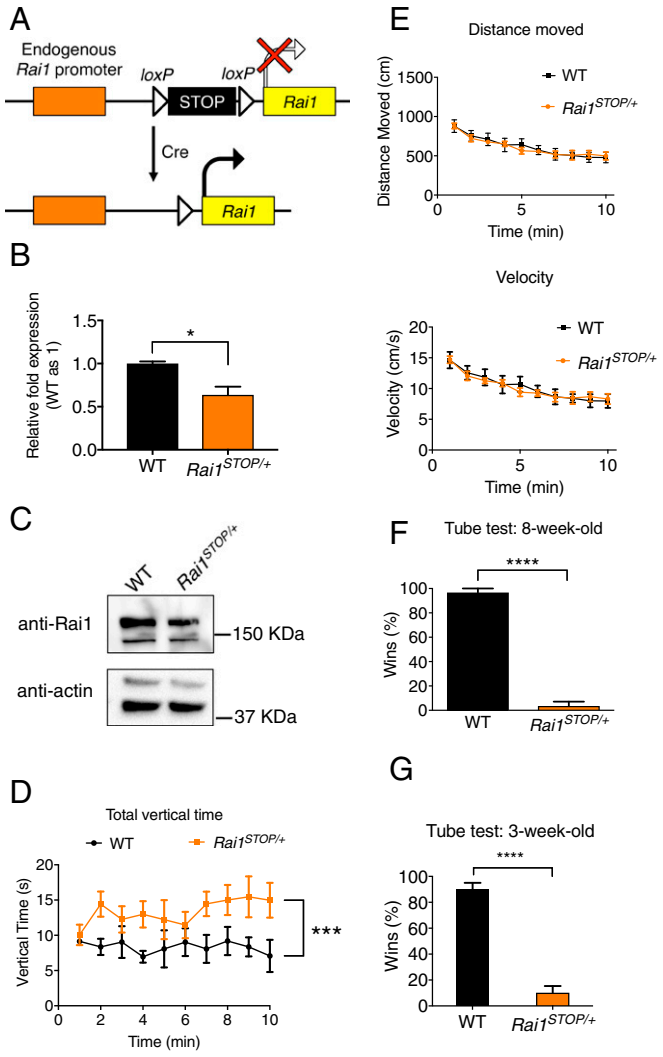

Fig. 1. $Rai1^{STOP/+}$ mice display increased rearing and social interaction deficits. (*A*) Schematic showing the strategy to conditionally reactivate *Rai1* expression. (*B*) Quantitative RT-PCR showing decreased *Rai1* mRNA expression in the $Rai1^{STOP/+}$ brains ($n = 3$; mean ± SEM; $^*P < 0.05$; *t* test). (*C*) Western blot showing a decreased Rai1 protein expression in the $Rai1^{STOP/+}$ brain. (*D*) $Rai1^{STOP/+}$ mice showed increased rearing in the activity chamber (mean ± SEM; $^{***}P < 0.001$; two-way ANOVA followed by Tukey post hoc test; for *D*–*F*, WT mice, $n = 5$; $Rai1^{STOP/+}$ mice, $n = 7$). (*E*) Travel distance and velocity in the activity chamber were not significantly different between WT and $Rai1^{STOP/+}$ mice (mean ± SEM; $P > 0.05$; two-way ANOVA). (*F*) $Rai1^{STOP/+}$ mice showed a severe social interaction deficit in the tube test (mean ± SEM; $^{****}P < 0.0001$; *t* test). (*G*) Juvenile $Rai1^{STOP/+}$ mice showed abnormal social interaction in the tube test ($n = 7$ for each genotype, mean ± SEM; $^{****}P < 0.0001$; *t* test).

In the activity chamber, $Rai1^{STOP/+}$ mice showed an increased stereotypical vertical activity (rearing) (Fig. 1*D*) while retaining an otherwise normal activity level (Fig. 1*E*). The time spent in the periphery and center of the activity chamber was not different between $Rai1^{STOP/+}$ and WT mice (*SI Appendix*, Fig. S1 *B* and *C*), suggesting a normal anxiety level. $Rai1^{STOP/+}$ mice showed normal motor coordination in the pole test and normal context- and cued-recalls in the fear-conditioning test (*SI Appendix*, Fig. S1 *D* and *E*). Furthermore, they retained normal spatial learning as shown by Y maze and Morris water maze (*SI Appendix*, Fig. S1 *F*–*H*). A hot plate test showed that $Rai1^{STOP/+}$ mice retained normal pain sensitivity (*SI Appendix*, Fig. S1*I*). These results are consistent with previous findings in $Rai1^{+/-}$ mice (12, 14).

One cardinal feature of ASD is abnormal reciprocal social interaction (15, 16). We used a tube test to measure social interaction by quantifying the encounters between two unfamiliar mice (17). When two mice are simultaneously released from opposing ends of a transparent tube, one mouse will eventually be pushed out or voluntarily retreat from the tube and be declared as the "loser" (*SI Appendix*, Fig. S1*J*). When performed on mice that share a cage, the tube test measures social hierarchy and dominance (18, 19). For unfamiliar mice that have not established social hierarchy, as in our case, the tube test reflects the willingness of stranger mice to maintain close physical proximity in a face-to-face social encounter (20). We found that $Rai1^{STOP/+}$ mice showed a dramatic defect in the tube test, losing ~90% of the matches to noncagemate WT mice (Fig. 1*F*), similar to a recent report for $Rai1^{+/-}$ mice (21). We previously found that 3-wk-old *Rai1* conditional knockout mice exhibit transcriptional misregulation in the brain (12). Accordingly, we tested the social interaction of $Rai1^{STOP/+}$ mice in the tube test at 3 wk of age and found a significant deficit (Fig. 1*G*). Importantly, performance in the tube test was independent for the weight or the locomotive activity in the open field (19).

To test if these neurobehavioral phenotypes are sexually dimorphic, we also tested female $Rai1^{STOP/+}$ mice. We found that female $Rai1^{STOP/+}$ mice showed normal horizontal activity in the activity chamber, increased rearing, abnormal social interaction in the tube test, and increased body weight (*SI Appendix*, Fig. S2 *A*–*D*). Thus, impaired social interaction is a robust and early onset phenotype consistent between male and female $Rai1^{STOP/+}$ mice.

Several lines of evidence suggest that aggression was not a major contributing factor to social interaction deficit from the tube test. First, both male and female $Rai1^{STOP/+}$ mice showed a similar social deficit in the tube test, yet it is known that females exhibit a low level of aggression (22). Second, 3-wk-old mice had not yet become aggressive toward their male conspecifics, yet 3-wk-old $Rai1^{STOP/+}$ mice already had shown a social interaction deficit. Third, we did not observe aggressive behavior for both 3-wk-old and adult mice during the tube test, consistent with previous findings that mice that won the tube test do not show increased aggression in the resident-intruder assay (18). Finally, we used age- and weight-matched mice for the tube test so these factors do not contribute to the results.

Partial Rescue of Transcriptional Deficits. To restore the Rai1 level in a temporally precise manner, we utilized an $Ubc^{CreERT2}$ allele that allows global Cre expression upon tamoxifen (TM) injection (23). To avoid the toxicity associated with consecutive TM injections (24), we established a regime of five TM treatments (100 mg/kg) over 10 d, which restored *Rai1* mRNA and protein expression of $Ubc^{CreERT2}$;$Rai1^{STOP/+}$ mice to WT level 10 d after the last injection (Fig. 2 *A*–*C*). Injection of vehicle (corn oil) did not result in nonspecific activation of *Rai1* (Fig. 2*B*).

Loss of *Rai1* affects the mRNA expression of hundreds of genes (12). We tested whether reinstatement of *Rai1* after symptom onset is sufficient to repair the transcriptome. Loss of *Rai1* results in behavioral symptoms (Fig. 1*G*) and transcriptional misregulation (12) at 3 wk of age. Therefore, we treated 3-wk-old WT, $Rai1^{STOP/+}$, and $Ubc^{CreERT2}$;$Rai1^{STOP/+}$ (hereafter, rescue) mice with TM and performed whole-transcriptome sequencing (RNA-seq) to examine their cortical transcriptomes at 4 mo of age ($n = 5$ for each genotype). When comparing WT and $Rai1^{STOP/+}$ cortices, we detected 792 differentially expressed genes (DEGs) with a false discovery rate adjusted P value < 0.05 and a $\log_2$ fold change >0.5 (*SI Appendix*, Fig. S3*A* and Dataset S1). Notably, *Rai1* reactivation significantly reduced the number of DEGs between WT and rescue mice (down to 356 genes, a 55% reduction) (*SI Appendix*, Fig. S3*A* and Dataset S2). We further performed hierarchical clustering to examine the expression pattern of individual DEGs across groups. Despite an early absence of *Rai1*, the DEG profile of the rescue mice clustered with WT littermates (Fig. 2*D*). Quantitative RT-PCR confirmed that *Rai1* reactivation normalized several misregulated genes that were also downregulated in our previous RNA-seq experiments (*SI Appendix*, Fig. S3*B*) (12). Principal component analysis using DEGs found that WT and $Rai1^{STOP/+}$ transcriptomes formed distinct clusters, and the transcriptomes of rescue mice occupied intermediate positions (Fig. 2*E*), suggesting at least a partial rescue at a genome-wide scale.

Next, we asked if the corrected genes belong to specific functional categories. Gene ontology (GO) analysis comparing WT and $Rai1^{STOP/+}$ DEGs indicated that pathways, including in nervous system development and neurogenesis, were significantly misregulated in the $Rai1^{STOP/+}$ brain (Fig. 2*F* and *SI Appendix*, Fig. S3*C*), consistent with our previous findings from *Rai1* conditional knockout mice (12). Notably, at 4 mo of age, pathways related to neurodevelopment were corrected by *Rai1* reactivation in the rescue mice (Fig. 2*F*). GO analysis using the DEGs detected in WT versus rescue mice also showed that genes involved in the cellular metabolic process were misregulated, suggesting that delayed *Rai1* reactivation did not fully rescue the transcriptomic difference between WT and $Rai1^{STOP/+}$ cortex. We noted that the 4-mo-old $Rai1^{STOP/+}$ cortex showed more pronounced transcriptional misregulation than what we previously found in the 3-wk-old $Nestin^{Cre}$;$Rai1^{CKO}$ cortex (*SI Appendix*, Fig. S3*D*), suggesting that the transcriptional deficits worsened with age. Thus, early reversal of the Rai1 level could hold more therapeutic promise. Together, restoration of Rai1 in juvenile symptomatic mice partially reversed the pathogenic transcriptional events in the neurodevelopmental pathways.

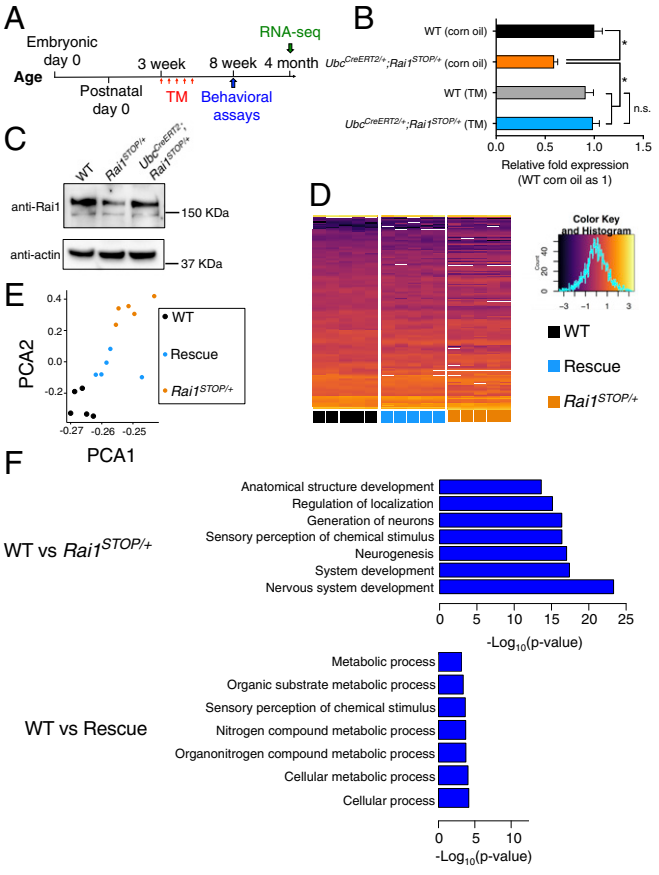

Fig. 2. Reactivation of *Rai1* in juvenile mice partially rescued transcriptional deficits. (*A*) Time line for TM injections, behavioral assays (Fig. 3), and RNA-seq experiments. (*B*) Quantitative RT-PCR showing that the Rai1 level was restored to the WT level in a Cre-dependent manner ($n = 3$; mean ± SEM; *$P < 0.05$, n.s., not significant; one-way ANOVA followed by Tukey post hoc test). (*C*) Western blot showing that decreased Rai1 protein level was normalized by TM treatment. (*D*) Hierarchical clustering of DEGs across genotypes, with each row representing individual genes and each column representing each sample (*Inset*: *x* axis represents the z-score; *y* axis represents the count in each bin of the histogram). (*E*) Principal component analysis of DEGs showing that the rescued transcriptomes move closer to WT transcriptomes. Each dot represents one mouse. (*F*) GO analysis using DEGs suggests that the genes involved in neurodevelopment were among the most misregulated in the $Rai1^{STOP/+}$ brains (for full lists, see *SI Appendix*, Fig. S3*A* and Datasets S1 and S2).

Rescue of Social Interaction Deficits by Restoring the Rai1 Level at Postnatal 3 Wk but Not 7 Wk. To test if transcriptional repairs are accompanied by functional rescue after reactivating *Rai1* at 3 wk of age, we performed behavioral assays at 8 wk of age. In the activity chamber, the rescue mice exhibited an intermediate level of activity compared with WT and $Rai1^{STOP/+}$ mice, although statistically indistinguishable from $Rai1^{STOP/+}$ mice (Fig. 3*A*). Other aspects of the locomotor and exploratory behaviors remained comparable between genotypes (*SI Appendix*, Fig. S4 *A*–*C*). Remarkably, while $Rai1^{STOP/+}$ mice consistently lose ∼90% of the matches against WT mice in the tube test, the rescue mice showed an equal winning rate against WT mice (Fig. 3*B*). Furthermore, the rescue mice won 86% of the matches against the $Rai1^{STOP/+}$ mice (Fig. 3*B*).

To investigate the nature of the social interaction deficit, we quantified the pattern of mouse interaction in the tube test by frame-to-frame scoring of the video blind to genotypes. We found that, in the WT vs. $Rai1^{STOP/+}$ social encounters, $Rai1^{STOP/+}$ mice voluntarily retreated more frequently than WT mice (*SI Appendix*, Fig. S4*D*). Rescue mice showed a retreat number similar to WT mice. When encountering $Rai1^{STOP/+}$ mice, rescue mice also showed a significantly lower retreat number (*SI Appendix*, Fig. S4*D*). Finally, WT, $Rai1^{STOP/+}$, and rescue mice all showed similar social preference for intruder mice over a novel object in a home cage social discrimination test (*SI Appendix*, Fig. S4*E*), suggesting that the social deficit was not due to the lack of social motivation. In summary, correlating with transcriptional repair, restoring the Rai1 level in symptomatic juvenile mice fully reversed the social interaction deficit in the tube test.

Prompted by the full reversal of the social interaction deficit in the $Rai1^{STOP/+}$ juvenile mice, we next normalized the Rai1 level by treating 7-wk-old male mice with TM and subjecting them to behavioral assays at 4 mo of age. We found that neither rearing (Fig. 3*C*) nor social interaction (Fig. 3*D*) were rescued, indicating that restoration of the Rai1 level in adult mice was insufficient to reverse the social interaction deficits of $Rai1^{STOP/+}$ mice.

Proper Social Interaction Requires a Correct *Rai1* Dose in both Excitatory and Inhibitory Neurons. *Rai1* is expressed in a multitude of cell types in the brain, including excitatory and inhibitory

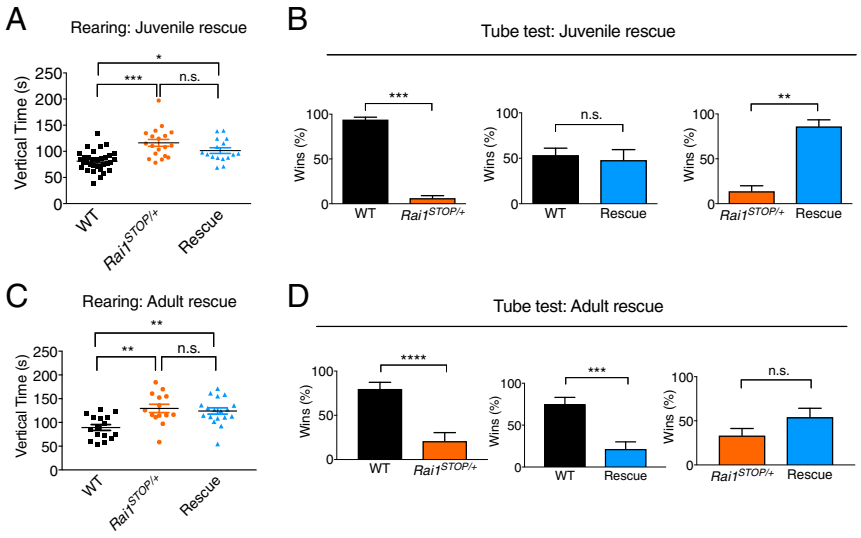

Fig. 3. Reactivation of *Rai1* in juvenile but not adult mice reversed social interaction phenotypes. (*A*) *Rai1* reactivation at juvenile age did not significantly rescue the rearing phenotype in 8-wk-old mice (mean ± SEM; $*P < 0.05$, $***P < 0.001$, n.s., not significant; two-way ANOVA followed by Bonferroni post hoc test). (*B*) *Rai1* reactivation at juvenile age fully reversed the abnormal social interaction of 8-wk-old mice in the tube test ($n = 22$ for WT mice, $n = 16$ for $Rai1^{STOP/+}$ mice, and $n = 13$ for rescue mice) (mean ± SEM; $**P < 0.01$, $***P < 0.001$, n.s., not significant; *t* test). (*C*) *Rai1* reactivation at adult stage did not rescue the rearing phenotype in 4-mo-old mice (mean ± SEM; $**P < 0.01$, n.s., not significant; two-way ANOVA followed by Bonferroni post hoc test). (*D*) *Rai1* reactivation at adult stage did not reverse the abnormal social interaction of 4-mo-old mice in the tube test ($n = 14$ for WT mice, $n = 12$ for $Rai1^{STOP/+}$ mice, and $n = 12$ for rescue mice) (mean ± SEM; $***P < 0.001$, $****P < 0.0001$, n.s., not significant; *t* test).

neurons (12). To test if restoring the Rai1 level in excitatory or inhibitory neurons alone is sufficient to correct the abnormal social interaction, we crossed $Rai1^{STOP/+}$ mice with $Vglut2^{Cre}$ or $Vgat^{Cre}$ mice and selectively normalized *Rai1* expression in excitatory or inhibitory neurons, respectively (*SI Appendix*, Fig. S5 *A* and *B*) (25). We found that both Vglut2-Rescue and Vgat-Rescue mice behaved similar to $Rai1^{STOP/+}$ mice (*SI Appendix*, Fig. S5*C*), suggesting that restoring Rai1 level in excitatory or inhibitory neurons alone was not sufficient to normalize social interaction.

In a complementary set of experiments, we deleted one copy of *Rai1* in excitatory and inhibitory neurons by crossing $Rai1^{flox/flox}$ mice (12) with $Vglut2^{Cre}$ and $Vgat^{Cre}$ mice and generated $Vglut2^{Cre}$;$Rai1^{flox/+}$ and $Vgat^{Cre}$;$Rai1^{flox/+}$ mice. We confirmed reduced *Rai1* expression in brain regions enriched with Cre-expressing neurons (*SI Appendix*, Fig. S5*D*). Similar to $Rai1^{+/-}$ mice, mice losing one copy of *Rai1* in $Vglut2^{Cre}$- or $Vgat^{Cre}$-expressing neurons showed a defective social interaction when encountering unfamiliar WT mice (*SI Appendix*, Fig. S5*E*). Interestingly, both $Vglut2^{Cre}$;$Rai1^{flox/+}$ and $Vgat^{Cre}$;$Rai1^{flox/+}$ mice won more matches when encountering $Rai1^{+/-}$ mice, suggesting that proper levels of *Rai1* expression in $Vglut2^{Cre}$- or $Vgat^{Cre}$-negative cells confer an intermediate phenotype (*SI Appendix*, Fig. S5*E*). Together, these data indicate that a proper dose of *Rai1* is required in both excitatory and inhibitory neurons to control social interactions. As a result, global (Fig. 3*A*) rather than restricted (*SI Appendix*, Fig. S5*C*) re-expression of *Rai1* is necessary to normalize social interaction abnormalities caused by *Rai1* haploinsufficiency.

Reduced Spine Density in Prefrontal Cortex Neurons. The medial prefrontal cortex (mPFC) is a critical region that controls social cognition in humans and mice (26). Mediodorsal thalamic input to the mPFC regulates social interaction in the tube test (18). In the rodents, the mediodorsal thalamic inputs predominantly synapse onto the apical dendritic trunk of layer V pyramidal cells located within layers II/III (27). To investigate whether *Rai1* haploinsufficiency results in structural changes of mPFC, we crossed $Rai1^{STOP/+}$ with $Thy1^{EGFP}$ (28) mice and quantified the spine density of layer V pyramidal neurons within layers II/III. We observed a significant reduction (~22.8%) of spine density in 1-mo-old $Rai1^{STOP/+}$;$Thy1^{EGFP}$ mice compared with age-matched $Rai1^{+/+}$;$Thy1^{EGFP}$ control littermates (Fig. 4 *A* and *B*). Subregions of the mPFC, including the anterior cingulate cortex (ACC) and the prelimbic cortex (PL), showed a consistent reduction of dendritic spines (Fig. 4*C*). The spine density phenotype was also more prominent in the anterior (~24% decrease for Bregma +2.2 to +2.8 mm) than in the posterior (~14% decrease for Bregma +1.9 to +2.2 mm) mPFC (Fig. 4*D*).

Optogenetic Activation of mPFC Neurons Partially Rescues Social Interaction Deficits. Optogenetic stimulation of the mPFC excitatory neurons has been shown to improve winning in the tube test (18). We therefore tested if activating mPFC can correct the

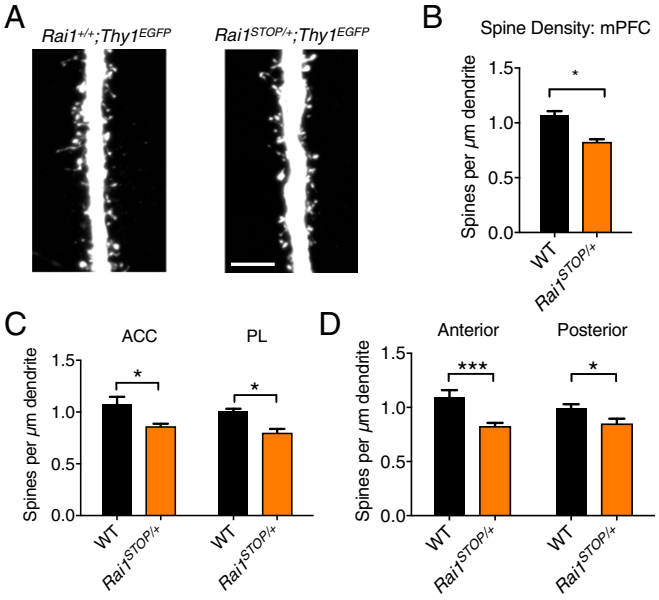

Fig. 4. Decreased dendritic spine density of mPFC neurons in $Rai1^{STOP/+}$ mice. (*A*) Representative image of WT ($Rai1^{+/+}$;$Thy1^{EGFP}$) and $Rai1^{STOP/+}$;$Thy1^{EGFP}$ main apical dendritic trunk of layer V pyramidal neurons at layers II/III. (Scale bar, 5 μm.) (*B*) $Rai1^{STOP/+}$ mice (three mice, $n = 124$ segments) showed a decreased dendritic spine density in the mPFC compared with their WT littermates (three mice, $n = 128$ segments; mean ± SEM; $*P < 0.05$; *t* test). (*C*) $Rai1^{STOP/+}$ mice showed decreased spine density in both ACC (WT, $n = 71$ segments; $Rai1^{STOP/+}$, $n = 68$ segments) and PL (WT, $n = 53$ segments; $Rai1^{STOP/+}$, $n = 60$ segments) compared with their WT littermates (mean ± SEM; $*P < 0.05$; *t* test). (*D*) $Rai1^{STOP/+}$ mice showed decreased spine density in both anterior mPFC (WT, $n = 60$ segments; $Rai1^{STOP/+}$, $n = 56$ segments) and posterior mPFC (WT, $n = 64$ segments; $Rai1^{STOP/+}$, $n = 72$ segments) compared with their WT littermates (mean ± SEM; $*P < 0.05$, $***P < 0.001$; *t* test). Anterior mPFC showed a greater loss of spine density.

social deficit in adult *Rai1*$^{STOP/+}$ mice (8–10 wk old). We stereotactically injected adeno-associated virus (AAV) containing humanized channelrhodopsin-2 under the control of human synapsin promoter (*AAV2-hSyn-hChR2(H134R)-EYFP*) into the right mPFC of adult *Rai1*$^{STOP/+}$ mice and implanted an optic fiber directly above the injection site (*SI Appendix*, Fig. S6 *A* and *B*). An AAV-encoding enhanced yellow fluorescent protein (EYFP) driven by the same promoter (*AAV2-hSyn-EYFP*) served as a control. We adopted two photostimulation protocols that have been shown to induce winning in the tube test: a 100-Hz phasic and a 5-Hz tonic protocol (*SI Appendix*, Fig. S6 *C* and *D*) (18). We confirmed that photostimulation significantly increased Fos expression in the channelrhodopsin-injected side (*SI Appendix*, Fig. S6*E*). We then performed a tube test by photostimulating both unfamiliar mice to rule out the potential visual effect of laser stimulation (Fig. 5*A*).

Under the laser-off control condition, WT-EYFP mice won more matches against both *Rai1*$^{STOP/+}$-EYFP (Fig. 5*B*) and *Rai1*$^{STOP/+}$-ChR2-EYFP mice (Fig. 5*C*), while *Rai1*$^{STOP/+}$-EYFP and *Rai1*$^{STOP/+}$-ChR2-EYFP mice behaved similarly (Fig. 5*D*). We then delivered 100-Hz phasic light to activate mPFC immediately before the mice entered the tube and throughout the match, which on average lasted 31.47 ± 7.26 s (n = 192 trials). Interestingly, photostimulation significantly increased winning of *Rai1*$^{STOP/+}$-ChR2-EYFP mice when encountering *Rai1*$^{STOP/+}$-EYFP mice (74.3 ± 6.5%, n = 8 mice for each genotype) (Fig. 5*D*). However, photostimulation did not affect encounters between *Rai1*$^{STOP/+}$-ChR2-EYFP and WT-EYFP mice (Fig. 5*C*), suggesting that activating mPFC alone does not restore all circuit deficits. This is consistent with *Rai1*$^{STOP/+}$-ChR2-EYFP mice showing an intermediate phenotype in between WT-EYFP and *Rai1*$^{STOP/+}$-EYFP mice. The 5-Hz tonic protocol had no impact on tube test performance in *Rai1*$^{STOP/+}$-ChR2-EYFP mice (*SI Appendix*, Fig. S6 *F–H*).

Finally, we quantified social encounters between *Rai1*$^{STOP/+}$-ChR2-EYFP and *Rai1*$^{STOP/+}$-EYFP mice during laser on-and-off paradigms. We found that mPFC activation reduced the average match duration (*SI Appendix*, Fig. S6*I*) and decreased the retreat number of *Rai1*$^{STOP/+}$-ChR2-EYFP mice (*SI Appendix*, Fig. S6*J*), suggesting an increased propensity to engage in social encounters. Collectively, these results provide evidence that circuit-level intervention can partially improve social interaction in adult *Rai1*$^{STOP/+}$ mice.

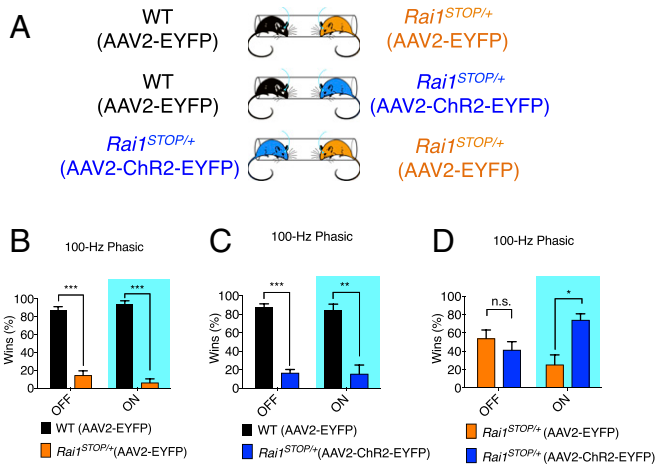

Fig. 5. Optogenetic activation of mPFC neurons partially corrected the social interaction phenotype of *Rai1*$^{STOP/+}$ mice. (*A*) Schematic for the tube test encounters. Mouse genotypes with the injected virus are indicated. Virus was injected at 8 wk of age and allowed to express for at least 1 mo. (*B*) Phasic photostimulation did not affect social interaction between WT-EYFP (n = 12) and *Rai1*$^{STOP/+}$-EYFP (n = 12) mice in the tube test (mean ± SEM; ***P < 0.001, t test). (*C*) Phasic photostimulation did not affect social interaction between WT-EYFP (n = 12) and *Rai1*$^{STOP/+}$-ChR2-EYFP (n = 12) mice (mean ± SEM; **P < 0.01, ***P < 0.001; t test). (*D*) Phasic photostimulation improved social interaction of *Rai1*$^{STOP/+}$-ChR2-EYFP (n = 12) when encountering *Rai1*$^{STOP/+}$-EYFP (n = 12) mice (mean ± SEM; *P < 0.05, n.s., not significant; t test).

Discussion

A key question in neurodevelopmental disorders such as ASDs is whether the symptoms are caused by early and irreversible defects during neural development or by disruption of potentially reversible defects in adult function (29). On the one hand, ASDs are typically diagnosed before 3 y of age (15), suggesting that ASD-causing genes regulate neural development. On the other hand, some ASD-causing genes have a continuous function throughout life. For example, syndromic autism genes such as *MeCP2* are required for adult neural functions (30), suggesting that the temporal window for treatment may extend well beyond early development. Studies using mouse models of syndromic ASDs have shown a range of reversibility. For example, adult restoration of *Syngap1* failed to reverse any behavioral phenotypes (31), highlighting the difficulty of reversing a congenital developmental disorder. In contrast, multiple disease features of Rett syndrome and *MECP2* duplication syndrome mouse models can be rescued by postsymptomatic normalization of MeCP2 levels (32, 33). Similarly, adult restoration of *Shank3* can rescue selective autistic-like symptoms in mice (24). Therefore, the reversibility of each disorder must be evaluated individually.

As an early onset syndromic ASD, the reversibility of SMS was previously unknown. Here, we uncovered a critical postnatal window to reverse social behavior deficits in a mouse model of SMS by normalizing the Rai1 level. Restoring the Rai1 level in early adolescence, after mice have already exhibited transcriptional and social interaction deficits, partially restores transcriptome and fully rescues the social interaction deficits. On the molecular level, delayed Rai1 restoration normalized the expression of Rai1 target genes involved in the functional development of the nervous system but not those involved in metabolic processes (Fig. 2*F*). This suggests that early Rai1 expression regulates specific neural developmental pathways. The inability of adult Rai1 re-expression to reverse behavioral deficits also suggests that the temporal window for Rai1 to normalize the transcriptional events causing social behavioral deficits closes during adolescence. Given the continuous expression of Rai1 in the adult brain (12), the functions of Rai1 in the mature nervous system remain unclear.

At the neural circuit level, we demonstrated that, even after that critical window (3–4 wk of age), optogenetic activation of mPFC provides an alternative treatment option to directly modulate neural circuit activity and correct the social interaction deficit. This suggests that the function of neural circuits underlying social interaction may not be permanently damaged by *Rai1* haploinsufficiency. It is possible that reduced spine density in the mPFC of *Rai1*$^{STOP/+}$ mice contributed to a decreased thalamic input important for social interaction in the tube test (18). The partial rescue effect of mPFC optogenetic activation likely partially overcame this defect. The partial rescue also suggests that loss of Rai1 causes neural defects in other brain regions and/or cell types. Supporting this notion, we found that both excitatory and inhibitory neurons depend on the proper Rai1 level to control social interaction. Identifying the Rai1-dependent inhibitory neurons will shed light on the neural mechanism underlying social interaction in the tube test.

The different therapeutic potential of Rai1 reactivation in adolescent and adult stages suggests that Rai1 has different roles in early development and adulthood. Interestingly, in a mouse model of PTLS that overexpresses Rai1 in the forebrain neurons (34), it was found that reducing the Rai1 level either before or after symptom onset was insufficient to prevent or reverse the

PTLS-like phenotypes. Therefore, SMS and PTLS likely have distinct critical windows for therapeutic interventions. Our work lays the groundwork for future therapeutic strategies for designing clinical trials for SMS and potentially other genomic disorders.

Materials and Methods

Animals. All animal procedures followed animal care guidelines approved by Stanford University's Administrative Panel on Laboratory Animal Care. F1 hybrids of C57BL/6J:129 and CD1 mice were used for all experiments. *Rai1*$^{STOP/+}$ mice were backcrossed onto a CD1 background for at least six generations, and all *Cre* mice were maintained in a C57BL/6J background. Mice were housed in groups on an inverted 12/12 h light/dark cycle with ad libitum access to food and water. The *Ubc*^{CRreERT2}, *Thy1*^{EGFP}, *Vgat*^{Cre}, and *Vglut2*^{Cre} mice were obtained from the Jackson Laboratory (23, 25, 28). *Rai1*$^{+/-}$ mice were generated by crossing the *Nestin*^{Cre} mice (which have sporadic germ-line activity) with the *Rai1*$^{flox/flox}$ mice (12), followed by breeding out the Cre allele.

Tamoxifen Treatment. Tamoxifen (T5648; Sigma) was dissolved in corn oil at a concentration of 20 mg/mL by vortexing and heating to 50 °C. Tamoxifen was protected from light by aluminum foil, aliquoted, and stored at −20 °C for no more than 2 wk. Each mouse received an i.p. 100 mg/kg tamoxifen injection every alternative day for 10 d (five doses).

Dendritic Spine Analysis. Mice were transcardially perfused with 4% paraformaldehyde and sectioned into 60-μm slices. Immunofluorescent staining was performed using chicken anti-GFP antibody (ab13970; Abcam) for 24 h followed by 2 h of room temperature secondary antibody staining (Jackson Immunoresearch). Confocal images of mPFC (the layers II/III of the main trunk of intact layer V pyramidal neurons) were taken with a 20× objective. Spine density is an underestimation due to the inability to count spines pointing toward or away from the imaging plane from the main apical dendritic trunk. Six slices per mouse brain, two to three cells per slice, and three dendritic apical trunk segments (~35 × 35 μm) per cell were imaged. Spine images were acquired from three mice per genotype. Spine counts from different anterior–posterior axes were used. All quantifications were done with the experimenter blind to the mouse genotypes. Statistical analysis was performed with Student's *t* test.

Tube Test. Animals used for the tube test were housed with mice with the same genotype and encountered unfamiliar mice in the tube test to avoid measuring social hierarchy established between cagemates. Mice were housed in cages in the testing environment for 1 d before training. In each of 2 training days, each mouse passed through the tube for 10 trials. In testing days, two mice of differing genotypes were placed at the two ends of the tube and released simultaneously to meet in the middle of the tube. The mouse that retreated first from the tube was designated as the loser. Experimenters were blinded to the genotypes of the mice in each trial. For the tube test using 3-wk-old mice, the diameter of the tube was reduced using clear vinyl so that the mice could not turn around. All mice participating in the tube test were of similar age and body weight.

Statistical Analysis. All data were statistically analyzed using Prism 7 (GraphPad) software, and *P* values less than 0.05 were considered significant. Statistical analysis was performed using Student's *t* test or one- or two-way ANOVA with Bonferroni's or Tukey's post hoc comparison.

ACKNOWLEDGMENTS. We thank the Stanford Transgenic Facility for generating the knock-in mice. This work was supported by grants from the Simons Foundation (SFARI Research Award 345098) (to L.L.) and from National Institute of Child Health and Human Development Grant 1K99HD092545-01 (to W.-H.H.). W.-H.H. was a Howard Hughes Medical Institute (HHMI) Fellow of the Jane Coffin Childs Memorial Research Fund. L.L. is a HHMI Investigator.

1. Carvalho CM, Lupski JR (2016) Mechanisms underlying structural variant formation in genomic disorders. *Nat Rev Genet* 17:224–238.
2. Neira-Fresneda J, Potocki L (2015) Neurodevelopmental disorders associated with abnormal gene dosage: Smith-Magenis and Potocki-Lupski syndromes. *J Pediatr Genet* 4:159–167.
3. Laje G, et al. (2010) Autism spectrum features in Smith-Magenis syndrome. *Am J Med Genet C Semin Med Genet* 154C:456–462.
4. Smith AC, et al. (1986) Interstitial deletion of (17)(p11.2p11.2) in nine patients. *Am J Med Genet* 24:393–414.
5. Slager RE, Newton TL, Vlangos CN, Finucane B, Elsea SH (2003) Mutations in RAI1 associated with Smith-Magenis syndrome. *Nat Genet* 33:466–468.
6. Girirajan S, et al. (2006) Genotype-phenotype correlation in Smith-Magenis syndrome: Evidence that multiple genes in 17p11.2 contribute to the clinical spectrum. *Genet Med* 8:417–427.
7. Potocki L, et al. (2000) Molecular mechanism for duplication 17p11.2- the homologous recombination reciprocal of the Smith-Magenis microdeletion. *Nat Genet* 24:84–87.
8. Treadwell-Deering DE, Powell MP, Potocki L (2010) Cognitive and behavioral characterization of the Potocki-Lupski syndrome (duplication 17p11.2). *J Dev Behav Pediatr* 31:137–143.
9. Zhang F, et al. (2010) Identification of uncommon recurrent Potocki-Lupski syndrome-associated duplications and the distribution of rearrangement types and mechanisms in PTLS. *Am J Hum Genet* 86:462–470.
10. De Leersnyder H (2006) Inverted rhythm of melatonin secretion in Smith-Magenis syndrome: From symptoms to treatment. *Trends Endocrinol Metab* 17:291–298.
11. Gropman AL, Duncan WC, Smith AC (2006) Neurologic and developmental features of the Smith-Magenis syndrome (del 17p11.2). *Pediatr Neurol* 34:337–350.
12. Huang WH, et al. (2016) Molecular and neural functions of Rai1, the causal gene for Smith-Magenis syndrome. *Neuron* 92:392–406.
13. Bi W, et al. (2005) Inactivation of Rai1 in mice recapitulates phenotypes observed in chromosome engineered mouse models for Smith-Magenis syndrome. *Hum Mol Genet* 14:983–995.
14. Bi W, et al. (2007) Rai1 deficiency in mice causes learning impairment and motor dysfunction, whereas Rai1 heterozygous mice display minimal behavioral phenotypes. *Hum Mol Genet* 16:1802–1813.
15. American Psychiatric Association (2013) *Diagnostic and Statistical Manual of Mental Disorders: DSM-5* (American Psychiatric Publishing, Inc., Washington, DC), 5th Ed.
16. de la Torre-Ubieta L, Won H, Stein JL, Geschwind DH (2016) Advancing the understanding of autism disease mechanisms through genetics. *Nat Med* 22:345–361.
17. Lindzey G, Winston H, Manosevitz M (1961) Social dominance in inbred mouse strains. *Nature* 191:474–476.
18. Zhou T, et al. (2017) History of winning remodels thalamo-PFC circuit to reinforce social dominance. *Science* 357:162–168.
19. Wang F, et al. (2011) Bidirectional control of social hierarchy by synaptic efficacy in medial prefrontal cortex. *Science* 334:693–697.
20. Tuttle AH, et al. (2017) Social propinquity in rodents as measured by tube cooccupancy differs between inbred and outbred genotypes. *Proc Natl Acad Sci USA* 114:5515–5520.
21. Rao NR, et al. (2017) Rai1 haploinsufficiency is associated with social abnormalities in mice. *Biology* 6:E25.
22. Takahashi A, Miczek KA (2014) Neurogenetics of aggressive behavior: Studies in rodents. *Curr Top Behav Neurosci* 17:3–44.
23. Ruzankina Y, et al. (2007) Deletion of the developmentally essential gene ATR in adult mice leads to age-related phenotypes and stem cell loss. *Cell Stem Cell* 1:113–126.
24. Mei Y, et al. (2016) Adult restoration of Shank3 expression rescues selective autistic-like phenotypes. *Nature* 530:481–484.
25. Vong L, et al. (2011) Leptin action on GABAergic neurons prevents obesity and reduces inhibitory tone to POMC neurons. *Neuron* 71:142–154.
26. Bicks LK, Koike H, Akbarian S, Morishita H (2015) Prefrontal cortex and social cognition in mouse and man. *Front Psychol* 6:1805.
27. Kuroda M, Murakami K, Kishi K, Price JL (1995) Thalamocortical synapses between axons from the mediodorsal thalamic nucleus and pyramidal cells in the prelimbic cortex of the rat. *J Comp Neurol* 356:143–151.
28. Feng G, et al. (2000) Imaging neuronal subsets in transgenic mice expressing multiple spectral variants of GFP. *Neuron* 28:41–51.
29. Krol A, Feng G (2018) Windows of opportunity: Timing in neurodevelopmental disorders. *Curr Opin Neurobiol* 48:59–63.
30. McGraw CM, Samaco RC, Zoghbi HY (2011) Adult neural function requires MeCP2. *Science* 333:186.
31. Clement JP, et al. (2012) Pathogenic SYNGAP1 mutations impair cognitive development by disrupting maturation of dendritic spine synapses. *Cell* 151:709–723.
32. Guy J, Gan J, Selfridge J, Cobb S, Bird A (2007) Reversal of neurological defects in a mouse model of Rett syndrome. *Science* 315:1143–1147.
33. Sztainberg Y, et al. (2015) Reversal of phenotypes in MECP2 duplication mice using genetic rescue or antisense oligonucleotides. *Nature* 528:123–126.
34. Cao L, et al. (2014) Correct developmental expression level of Rai1 in forebrain neurons is required for control of body weight, activity levels and learning and memory. *Hum Mol Genet* 23:1771–1782.